Membrane fractioning of pre-treated waste activated sludge for the recovery of valuable biocompounds

Nunez Diaz, Daniel; Oulego, Paula; Fini, Mahdi Nikbakht; Muff, Jens; Collado, Sergio; Riera, Francisco A.; Díaz, Mario

Published in:
Journal of Water Process Engineering

DOI (link to publication from Publisher):
10.1016/j.jwpe.2023.104086

Publication date:
2023

Document Version
Publisher's PDF, also known as Version of record

Journal of Water Process Engineering 55 (2023) 104086

Contents lists available at ScienceDirect

Journal of Water Process Engineering

journal homepage: www.elsevier.com/locate/jwpe

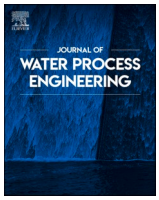

Membrane fractioning of pre-treated waste activated sludge for the recovery of valuable biocompounds

Daniel Núñez [a], Paula Oulego [a], Mahdi Nikbakht Fini [b], Jens Muff [b], Sergio Collado [a], Francisco A. Riera [a], Mario Díaz [a,*]

[a] Department of Chemical and Environmental Engineering, University of Oviedo, c/Julián Clavería 8, 33006 Oviedo, Spain
[b] Department of Chemistry and Bioscience, Aalborg University Esbjerg, Niels Bohrs Vej 8, Esbjerg 6700, Denmark

ARTICLE INFO

Keywords:
Biomolecules
Modelisation
Ultrafiltration
Waste valorisation
Wet oxidation

ABSTRACT

The recovery of added-value biocompounds from waste activated sludge (WAS) is a promising alternative to its current management. In this study, WAS was partially wet oxidised producing a highly complex stream mainly composed of humic acids, proteins and carbohydrates. This stream was ultrafiltered to assess the influence of membrane material and molecular weight cut-off (MWCO) on its fractioning based on the different sizes of the biomolecules contained in the oxidised WAS.

Flat-sheet polyethersulfone (PES), permanently hydrophilic polyethersulfone (PESH), and polyacrylonitrile (PAN) membranes with a MWCO of 50 KDa were evaluated. The best performance was obtained with PES membrane, achieving high retention values (around 70 % for proteins and carbohydrates, and 47 % for humic acids) and high differences in selectivity between proteins and carbohydrates with humic acids (around 23 %). For the size fractioning experiments, PES membranes of 10 and 3 kDa (PES10 and PES3) were used, obtaining the best results when filtering the PES50 membrane permeate with the PES3 membrane, retaining 83 % of carbohydrates, 87 % of proteins and 69 % of humic acids. These results open the possibility of separating carbohydrates, proteins and humic acids through an integrated membrane process.

Besides, membranes were characterized by atomic force microscopy, infrared spectroscopy, and contact angle measurements.

Multiple fouling models were assessed, and the main fouling in PAN membrane, and to a lesser extent in PES, was reversible. Conversely, PESH membrane fouling had a strongly irreversible character. Cake filtration can be considered the main fouling mechanism in all experiments.

1. Introduction

The biorefining of biowastes has been proposed as a sustainable means of waste valorisation, obtaining energy and biochemical resources while the volume of final waste is reduced [1]. Although it is yet at its conceptual phase [2], the steady rising trend of the biorefinery market value, expected to show an annual growth of 2.2 % until reaching a total value of USD 52680 million by 2027 [3], is a reliable marker for its potential. Waste activated sludge (WAS) is a promising raw matter for biorefinery, as it is a source of biomolecules (proteins, lipids, carbohydrates, humic acids and enzymes), phosphorus, bioplastics, bio-pesticides and also energy [4–10]. The current global market size of just the biomolecules present in WAS is of almost USD 200 billion, turning its recovery economically appealing [11].

WAS mainly consists of flocs of bacterial cells, which are formed by weak physical chemical interactions with extracellular polymeric substances [12] (a complex mixture of polymers generated by bacterial excretion, released after cell lysis or present in the incoming wastewater [13]). Thus, in order to recover the above-mentioned biocompounds, a prior solubilisation of the sludge is needed in order to break both the structure formed by the extracellular polymeric substances and the cell walls, thus releasing their intracellular content to the liquid medium. Several solubilisation methods have been tested for WAS, including ultra-sonication [14,15], cavitation [16], alkali treatment [15,17], ozonolysis [18], wet oxidation (WO) and thermal hydrolysis [19]. Among these techniques, WO is particularly interesting, due to its feasibility to be used at an industrial scale for sludge stabilisation [20].

It should be noted that this solubilisation results in a complex matrix,

* Corresponding author.
E-mail address: mariodiaz@uniovi.es (M. Díaz).

https://doi.org/10.1016/j.jwpe.2023.104086
Received 19 December 2022; Received in revised form 3 July 2023; Accepted 22 July 2023
Available online 4 August 2023

where interactions between the different released biomolecules can difficult their purification. For instance, electrostatic interactions between proteins and humic acids occur while binding to heavy metals such as Cu^{2+}, Zn^{2+}, and Cd^{2+} [21]; and even aggregates are formed when complexed with Cu^{2+} [22], hindering a suitable separation of these molecules by immobilised metal affinity chromatography. Besides, a selective precipitation is also not possible from this complex matrix, as proteins, carbohydrates and humic acids co-precipitate with several precipitation methods [19]. These molecules have important industrial applications separately: proteins are used in cosmetics, food industry, pharmaceuticals and animal feed; humic acids can be applied in agriculture, pharmaceuticals or ecological remediation, among other uses; and carbohydrates are often used in the food industry [11]. Thus, their separation is of great interest for the incorporation of WAS as a valuable raw material in a context of circular economy. Besides, lipid recovery for its use as biofuel from WAS faces difficulties during its purification with solvent extraction, as other lipidic contaminants such as wax esters, terpenoids and polycyclic aromatic hydrocarbons are extracted together with the desired lipids [4].

For these reasons, fractioning the solubilised WAS would improve the efficiency of further separation and purification steps. To that end, membrane filtration is a suitable technology for this purpose due to its advantages, such as high selectivity, low energy consumption, low cost, and mild operating conditions [23]. Nevertheless, the performance of the membrane filtration is affected by several factors, especially the choice of membrane material and its molecular weight cut-off (MWCO) [24–26]. Most membranes are polymeric, and the choice of this polymer is critical for the efficiency of the operation, since it affects the permeability rate, the separation ability or the fouling process, key parameters in the filtration process [23].

Despite their utter importance, polymeric materials have not yet been studied for the filtration of solubilised WAS, and the effect of MWCO has been scarcely studied. Hence, only Li et al. have tested the use of 1, 10, 30, and 50 kDa polysulphone membranes to concentrate humic acids [27,28]. Therefore, the objective of this work was to study the influence of the membrane material and MWCO on the fractionation of hydrothermally solubilised WAS in order to separate carbohydrates, proteins, and humic acids based on their size differences aiming to obtain partially purified streams of these compounds. In this sense, 3 different polymeric materials: polyethersulphone, hydrophylic polyethersulphone and polyacrylonitrile, with a MWCO from 3 KDa to 50 KDa, were evaluated, paying special attention to fouling modelling. Hydrophilic polyethersulfone and polyacrylonitrile have a hydrophilic character, unlike polyethersulfone, which is a hydrophobic material. Besides, an integrated membrane process for the recovery of biomolecules from WAS was also proposed.

2. Experimental

2.1. Oxidised waste activated sludge

Waste activated sludge was collected from the thickening unit of a wastewater treatment plant located in northern Spain (Baíña, Asturias). The collection was performed by trained plant personnel to ensure the representativeness of the samples. WAS was immediately solubilised by a partial WO at 160 °C and 40 bar for 80 min. These oxidation conditions were selected to maximise the production of the target molecules: if the intensity of the treatment is too high, the target molecules get oxidised or mineralised; if the intensity is too low, the sludge does not completely solubilise [29]. Additionally, as the oxidation intensity increases, the particle size decreases, reducing the retention capabilities of the membranes. A constant flow of 1200 mL/min of O_2 saturated with steam was maintained during the entire reaction. The content of the reactor was kept stirring at 150 rpm. A more detailed description of the reactor can be found in [30]. After the reaction, the oxidised WAS was centrifuged in order to work with the liquid phase. Sodium azide 0.1 % (w/v) was added to the oxidised WAS in order to prevent microbiological growth. The oxidised sludge was stored at 4 °C for 15 days and then replaced with fresh oxidised sludge.

2.2. Membrane filtration

2.2.1. Membranes

MQ (Synder Filtration) polyethersulfone (PES), UH050 (Microdyn Nadir) hydrophylic polyethersulfone (PESH), and MW (Suez) polyacrylonitrile (PAN) flat-sheet membranes with MWCO of 50 kDa (named as PES50, PESH50, and PAN50, respectively) were employed to perform the material screening experiments. Additionally, ST (Synder Filtration) and VT (Synder Filtration) PES flat-sheet membranes with MWCO of 3 and 10 kDa, respectively (named as PES3 and PES10), were used for the cut-off size screening experiments. All membranes were cut to a circular shape of 9 cm of diameter, and a filtration area of 63.62 cm^2.

Membrane hydrophilicity was characterized by contact angle measurements. The images were obtained with a CAM 200 optical contact angle meter (KSV Instruments Ltd., Finland). Sessile water droplets were dropped on the clean and fouled membrane surfaces using a syringe and let to spread freely. Images of the droplets were taken by a high-resolution CCD camera at 40 ms intervals for the first 0.36 s, and at 1 s intervals for the subsequent 19 s. Equilibrium sessile drop contact angles were determined from the steady-state angles using the KSV CAM 200 software by measuring the angle between the baseline of a liquid drop and the tangent at the solid–liquid boundary. All contact angle measurements were performed in triplicate using three different membrane samples.

2.2.2. Equipment and filtration conditions

Filtration experiments were carried out in duplicate using an FT17 Cross-flow Filtration Unit (Armfield Ltd., United Kingdom), which allows to perform tangential flow filtrations with flat sheet membranes. Prior to conducting the experiments, all polymeric membranes were preconditioned by running the equipment with no pressure for 30 min using distilled water. Subsequently, water was filtered under the operational conditions (indicated below) for an additional 30 min. The flux obtained in this sted was considered as the flux at $t = 0$. The permeate flux of the clean membranes was measured during this step for further fouling modelling. All the material screening filtration experiments were performed under the following conditions: temperature of 50.0 ± 0.4 °C, transmembrane pressure (TMP) of 4.0 ± 0.2 bar and crossflow velocity (CFV) of 3.00 m/s. The oxidised WAS was filtrated without permeate recirculation until a volume concentration rate (VCR) of 2.5 was reached.

During the MWCO screening experiments, the oxidised WAS was filtered with the PES50, PES10 and PES3 membranes. Besides, in order to assess the viability of the fractioning of the oxidised WAS, the permeate obtained after the filtration with PES50 was subsequently filtered with the PES10 or with the PES3 membranes, naming these permeates as PES50-10 and PES50-3, respectively. The experiments were performed under the same conditions than those used in the material screening ones. Only for obtaining the PES50-3 permeate, pressure was set at 30 bar and a VCR value of 1.25 was achieved.

Permeate flow was determined by gravimetric measurements of the permeate, which were collected automatically by the FT17 Cross-flow Filtration Unit software. Flux was calculated by the following equation (Eq. (1)):

$$J = \frac{Q_P}{A_M} \quad (1)$$

Where J is the permeate flux ($m \cdot s^{-1}$), Q_P is the permeate flow ($m^3 \cdot s^{-1}$), and A_M is the membrane surface area (m^2).

In addition, samples of the permeate and retentate were collected periodically and kept at 4 °C for further analysis.

After the filtrations, the fouled membrane was rinsed with distilled water until a constant flux was obtained, and its permeability was measured for further fouling modelling.

2.2.3. Fouling modelling

Resistance-in-series, Hermia's, and Mentha's fouling models were employed to characterise both the reversibility and main mechanism of membrane fouling occurred during the different filtration experiments.

Resistance-in-series model expresses the total hydraulic resistance of the membrane (R_T, m^{-1}) as the sum of different resistances caused by reversible fouling (R_{rev}, m^{-1}), irreversible fouling (R_{irrev}, m^{-1}), or by the membrane itself (R_m, m^{-1}) (Eq. (2)). Hydraulic resistance can be calculated as shown in Eq. (3):

$$R_T = R_m + R_{rev} + R_{irrev} \quad (2)$$

$$R = \frac{TMP}{\mu J} \quad (3)$$

Where μ is the dynamic viscosity of the WAS at 50 °C ($kg{\cdot}m{\cdot}s^{-1}$). By adding or subtracting the resistances obtained with the clean, fouled, or rinsed membrane fluxes, R_m, R_{rev}, and R_{irrev} can be easily calculated. A more detailed explanation of these calculations can be found in the Appendix of [31]).

The main fouling mechanism occurred on each membrane during ultrafiltration was determined through Hermia's model [32] (Eq. (4)):

$$\frac{dJ}{dt} = -K_j{\cdot}(J - J_0){\cdot}J^{2-n} \quad (4)$$

Where t is time (min), K_j is the model constant that depends on the fouling phenomenon, J_0 is the limiting flux ($m{\cdot}s^{-1}$), and n is a constant that varies for the fouling mechanism: complete pore blocking (CPB) ($n = 2$, K_b in min^{-1}), where the active membrane area is blocked by particles larger than the pore size; internal pore blocking (IPB) ($n = 1.5$, K_i in m^{-1}), where membrane pores are blinded by either adsorption or deposition of particles smaller than the pore size; particle pore blocking (PPB) ($n = 1$, K_p in m^{-1}), where particles might seal a pore over time, or bridge it and not block it completely; and cake filtration (CF) ($n = 0$, K_c in $min{\cdot}m^{-2}$), where a cake of particles that does not enter the pores is formed on the membrane surface [33].

The K_j for the four models were calculated by minimizing the difference between the predicted values and the experimental data, calculated as the sum of squared residuals (SSR). The model with the lowest SSR was chosen as the most suitable one for each set of experimental data.

In addition, flux was also modelled using the Mehta's model [34], which takes into account the two flux decline domains that take place during membrane filtration: domain 1, where a rapid flux decline occurs during the early stage of filtration; and domain 2, where the flux decline decreases until the flux remains quasi-stable [35]. It can be expressed as follows (Eq. (5)):

$$J = J_0 - J_{\infty 1}{\cdot}exp^{-\alpha t} + (J_{\infty 1} - J_{\infty 2}){\cdot}exp^{-\beta t} + J_{\infty 2} \quad (5)$$

Where $J_{\infty 1}$ is the flux at the end of domain 1 ($m{\cdot}s^{-1}$); $J_{\infty 2}$ is the flux at the end of domain 2 (i.e., at the end of the experiment) ($m{\cdot}s^{-1}$); and α ($min-1$) and β ($min-1$) are two constants determined experimentally that describe the rate of flux decline associated with the membrane fouling and the concentration polarization and gel layer formation, respectively.

2.3. Atomic force microscopy

The roughness of the fouled and clean membranes was analysed by atomic force microscopy (AFM). All AFM measurements were performed at room temperature (20 °C) using a Nanoscale scanning tunnelling microscope (Nanotec Cervantes FullMode SPM), working in contact mode in air medium with gold coated silicon nitride tips. Membrane samples were fixed to the sample holder of the microscope with high-vacuum silicone grease. Roughness parameters were determined from the collected data using the WSxM 5.0 software [36]. Membrane roughness was compared in terms of mean roughness (R_a [nm/μm]), root mean square roughness (rms), peak-to-peak distance (nm/μm), and surface skewness and kurtosis. R_a is the mean value of the surface relative to the centre plane; rms is the standard deviation of the heights for all the pixels in the image from the arithmetic mean [37]; and skewness and kurtosis describe the shape of a probability distribution, reflecting the obliquity and the flatness of the curve, respectively [38].

2.4. Infrared spectroscopy

Infrared spectra (FTIR) of the clean and fouled membranes were taken in the range from 600 to 4000 cm^{-1} using Varian 670-IR FTIR spectrometer equipped with a Golden Gate horizontal attenuated total reflectance (ATR) accessory. Experimental conditions were 32 scans, 4 cm^{-1} resolution and aperture open.

2.5. Analytical methods

Proteins, humic acids, carbohydrates, colour number (CN) and chemical oxygen demand (COD) were measured by colorimetric methods. Proteins and humic acids were measured following the modified Lowry method described by Frølund et al. [39], using bovine serum albumin and commercial humic acid as standards. Carbohydrates were measured according to the Dubois method [40] using D-glucose as standard. Spectral absorbance coefficients (SAC [cm^{-1}]) were measured at 436, 525 and 620 nm and used to calculate the CN value (cm-1) according to Eq. (6):

$$CN = \frac{SAC_{436}^2 + SAC_{525}^2 + SAC_{620}^2}{SAC_{436} + SAC_{525} + SAC_{620}} \quad (6)$$

The absorbances of proteins, humic acids, carbohydrates and SAC were measured with a Helios Alpha UV–Vis spectrophotometer (Thermo Scientific, USA).

Density was measured at 50 °C and 1 atm with a pycnometer. Kinematic viscosity was measured at 50 °C and 1 atm with a Cannon-Fenske inversed-flow viscometer (Proton, UK). Dynamic viscosity was calculated by multiplying the kinematic viscosity by the density. pH was measured with a Basic 20 pH meter (Crison, Spain). COD values were determined by the potassium dichromate method [41], and the absorbance at 600 nm was measured with a HACH DR/2500 spectrophotometer (Hach Company, USA). Total organic carbon (TOC) was determined with a Shimadzu TOC-V_{CSH} TOC analyser (Shimadzu, Japan).

Rejection coefficients (RC_i) were calculated according to the Eq. (7):

$$RC_i = 1 - \frac{C_{P_m,i}}{C_{R_t,i}} \quad (7)$$

Where $C_{P_m,i}$ and $C_{R_t,i}$ the concentration of the compound "i" in the permeate and the retentate ($g{\cdot}L^{-1}$), respectively. All analytical measurements were conducted at least three times.

3. Results and discussion

3.1. Oxidised waste activated sludge

The oxidised WAS was slightly acid and presented a deep brown colour. Its main physical-chemical characteristics are shown in Table 1.

Table 1
Main physical-chemical characteristics of the oxidised waste activated sludge.

Parameter	Value
pH	5.04 ± 0.03
COD[a] (g O_2 L^{-1})	20.5 ± 0.5
TOC[a] (g L^{-1})	8.00 ± 0.01
CN[a] (cm^{-1})	3.9 ± 0.2
Proteins (g L^{-1})	3.4 ± 0.3
Humic acids (g L^{-1})	8.4 ± 0.2
Carbohydrates (g L^{-1})	2.75 ± 0.03

[a] COD: chemical oxygen demand; TOC: total organic carbon; CN: colour number.

3.2. Membrane material screening

3.2.1. Contact angle measurements

Measured contact angles of water on the polymeric membranes used in the ultrafiltration of the oxidised WAS are shown in Table 2. A selection of the pictures of the sessile drops, from which the contact angles were calculated, can be found in Fig. A1.

A surface is considered hydrophilic if the contact angle is lower than 90° [42]. Thus, PES50 could be considered hydrophobic, while PESH50 and PAN50 were found to be hydrophilic. This was in accordance with the results obtained by other authors related to fouling resistance of ultrafiltration membranes [43]. After filtering the oxidised WAS, the fouled PES50 and PESH50 turned more hydrophilic than the pristine ones, while PAN50 became less hydrophilic after being fouled, which showed the different nature of the foulant-membrane interactions depending on the membrane material: it seems that PES50 and PESH50 were coated with more hydrophilic foulants, while PAN50 interacted with foulants less hydrophilic than itself.

3.2.2. Permeability tests

The fluxes obtained with PES50, PESH50 and PAN50 are shown in Fig. 1.

Final fluxes approximately 3 times higher were obtained with PESH50 (67.2 ± 0.9 LMH) and PAN50 (74 ± 3 LMH) compared to the one achieved by PES50 (25 ± 2 LMH), due to their hydrophilic character. In this sense, membrane hydrophilicity prevented fouling, in accordance to what was reported by other authors [44,45]. The resistance-in-series models (Fig. 2) confirmed the aforementioned about hydrophobicity and its higher tendency to fouling. In this sense, all the resistances (membrane, reversible and irreversible) measured for PES50, which added up a total hydraulic resistance of $1.07 \cdot 10^{14}$ m^{-1}, were higher than those of PESH50 (13.3, 2.5 and 1.1 times higher, respectively) and PAN50 (3.4, 2.4 and 6.3 times higher, respectively). On the other hand, the different behaviour between fluxes in PESH50 and PAN50 can be explained based on the values of irreversible fouling for each membrane. Thus, the resistance-in-series modelling showed that the higher tendency to fouling observed in PESH50 is due to irreversible fouling, since its R_{irrev} accounted for the 49.6 % of its total hydraulic resistance, while R_{irrev} observed in PAN50 only represented 12.4 % of the total hydraulic resistance. The total R_{irrev} also seemed to be correlated with the hydrophobicity of the membrane, as PES50 showed the highest R_{irrev} ($[2.8 \pm 0.4] \cdot 10^{13}$ m^{-1}), followed by PESH50 ($[2.45 \pm 0.01] \cdot 10^{13}$ m^{-1}) and PAN50 ($[4.3 \pm 0.6] \cdot 10^{12}$ m^{-1}).

Besides, reversible fouling was found to be the main fouling in PES50 and PAN50 membranes, corresponding to a 53.4 % and to a 68.9 % of the total fouling for PES50 and PAN50, respectively.

The fluxes obtained in this study were in the same order of magnitude than those obtained by other authors when PES membranes were used during the filtration of milk [46], refinery and petrochemical wastewater [47] and oil-in-water emulsion [48,49]; and with PAN membranes when tap water [50] and oil-in-water emulsion [49] were filtered. Besides, lower initial fluxes were obtained when PESH membranes were employed for the filtration of molasses [51], while similar fluxes were attained for olive oil washing wastewater [52].

It should be noted that the higher fluxes obtained with PESH50 and PAN50 come along with lower rejection coefficients and lower selectivities between proteins and humic acids (Table 3). In particular, the lowest rejection coefficients for CN, TOC, and the three measured biocompounds were those corresponding to PESH50. On the other hand, the highest rejections were obtained with PES50, also achieving the highest rejection differences between proteins and humic acids (22 % difference vs 7 % difference obtained with PAN50, and 10 % difference obtained with PESH50); and between carbohydrates and humic acids (23 % difference vs 13 % obtained with PAN50 and 17 % difference obtained with PESH50).

These higher retentions may be due to the formation of a thicker cake layer on top of the membrane, which would act as a secondary filtration mesh, increasing the selectivity of the membrane [53]. The formation of this thicker fouling cake could be observed through the resistance-in-series model (Fig. 2), where the R_{rev}, mainly associated with the formation of the fouling cake [54], was more than two-fold higher after filtering with PES50 ($[5.7 \pm 0.8] \cdot 10^{13}$ m^{-1}) than with PESH50 ($[2.3 \pm 0.2] \cdot 10^{13}$ m^{-1}) or PAN50 ($[2.41 \pm 0.07] \cdot 10^{13}$ m^{-1}). Rejection differences between PESH50 and PAN50 are coherent with this explanation, as the R_{rev} of PESH50 is slightly lower than that of PAN50.

As both higher rejection coefficients and higher rejection differences between humic acids and the other biomolecules (proteins and carbohydrates) were achieved with PES50, the fractionation tests with membranes of different MWCO (MWCO screening experiments) was carried out with PES membranes.

3.2.3. Flux modelling

As it can be seen in Fig. 3 and Table 4 (SSR), CF was the best-fitting Hermia's model in all three cases, although the fittings indicated that none of the Hermia's models fully explain the fouling mechanism, thus indicating several fouling mechanisms may have occurred throughout the filtration. Indeed, the fact that different fouling mechanisms occur at different stages of the filtration is well documented in the literature [55,56] and it was taken into account by Mehta's model [34]. Thus, CF was the main fouling mechanism overall, although irreversible pore blocking also occurred; especially during the filtration with PESH50, where the IPB model showed better fitting than in the filtrations with PES50 and PAN50, reflecting the above-mentioned more irreversible nature of the PESH50 fouling. Besides, CF has also been described by other authors as the main fouling mechanism of natural organic matter during ultrafiltration with PES membranes [57,58].

However, it should be noted that the best fitting of the experimental data was achieved with Mehta's model, which provides information about the effect of membrane fouling (parameter α) and concentration polarization and gel layer formation (parameter β) on the flux decline. The optimised values for these two constants are shown in Table 4. Higher α and β values represent faster initial membrane fouling and faster stabilisation of the flux by the establishment of the concentration polarization gradient and gel layer formation, respectively. The α values obtained for the filtrations with PESH50 and PAN50 were 10-fold higher than those of PES50 (3.88), while the β values were 4-fold lower than those obtained for PES50 ($5.20 \cdot 10^{-2}$). This indicates that a strong initial membrane fouling occurred after starting the filtration of the oxidised

Table 2
Water surface contact angles on the studied membranes.

Membrane size	Membrane material	Membrane state	Contact angle
50 kDa	PES	Clean	90 ± 3
		Fouled	70 ± 2
	PESH	Clean	72 ± 1
		Fouled	54 ± 11
	PAN	Clean	39 ± 4
		Fouled	57 ± 10

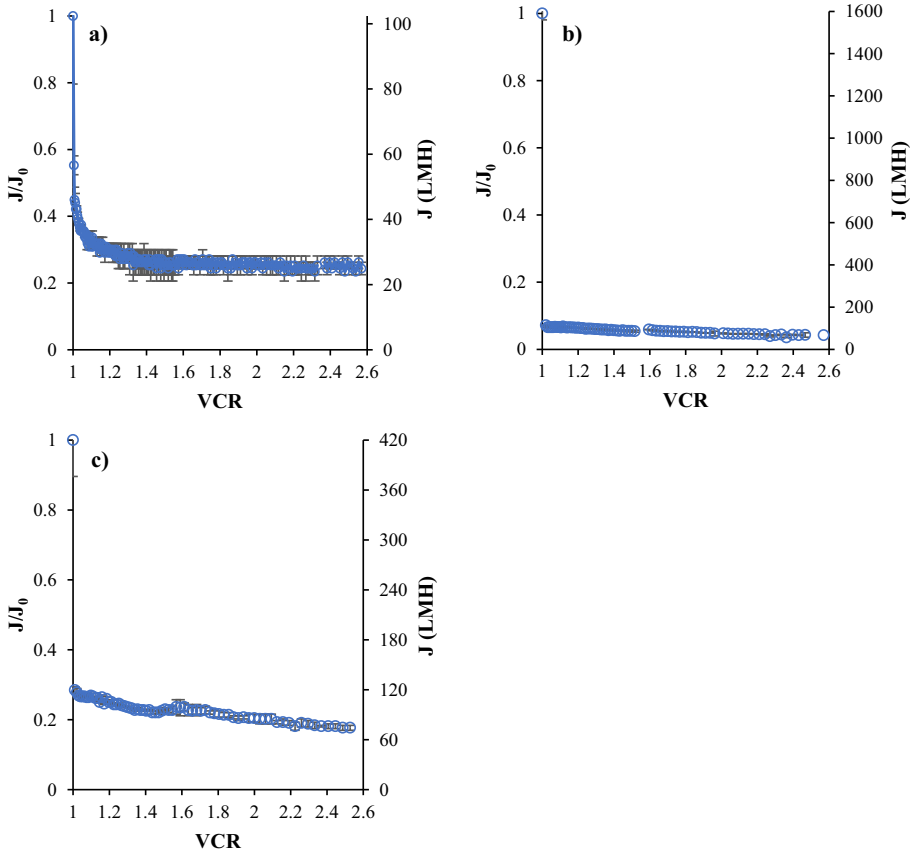

Fig. 1. Normalised flux variation over VCR for the oxidised WAS filtration with (a) PES50 (J_0 = 102.4 ± 0.2 L/m^{2}h), (b) PESH50 (J_0 = 1590 ± 40 L/m^{2}h) and (c) PAN50 (J_0 = 420 ± 40 L/m^{2}h).

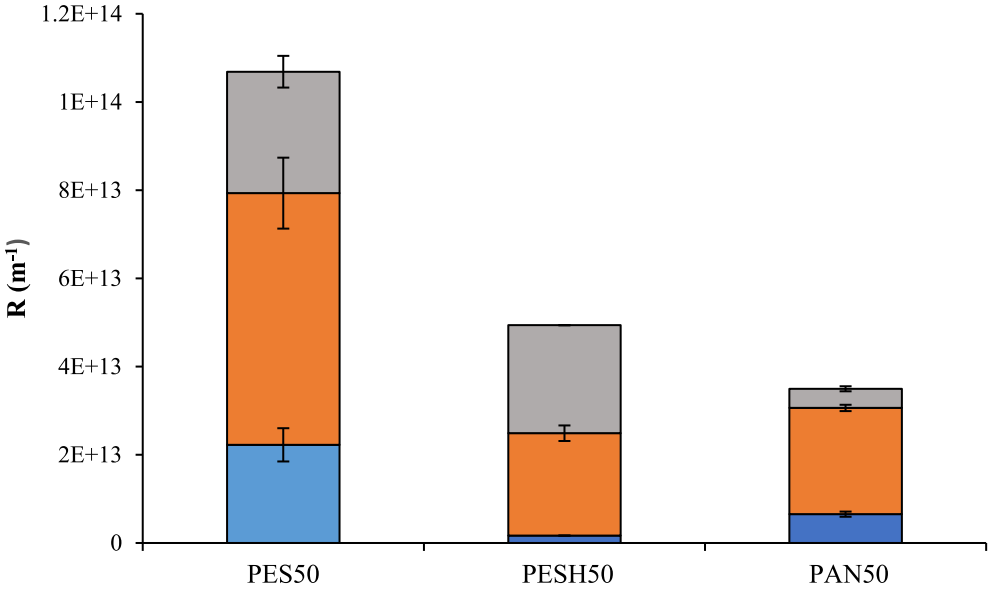

Fig. 2. R_m (■), R_{rev} (■) and R_{irrev} (■) after filtration with PES50, PESH50 and PAN50.

WAS with PESH50 and PAN50, causing a rapid decrease in the flux. After this initial drop, the stabilisation of the flux by concentration polarization occurred more slowly. Regarding the behaviour during the filtration with PES50, it was opposite to that of the other polymeric membranes: the initial drop caused by membrane fouling was less drastic, and the equilibrium in concentration polarization was reached faster.

This result is in accordance with the literature, and can be explained considering the polarization sieving model [59], based on the differences of hydrophilicity between the membranes:

Thus, in hydrophilic membranes, an initial irreversible adsorption layer is formed, regardless of the solute concentration, and subsequent

Table 3
Rejection coefficients (RC) obtained with the 50 kDa polymeric membranes.

	PES50*	PESH50*	PAN50*
RC_{CN*}	0.80 ± 0.02	0.69 ± 0.03	0.73 ± 0.04
RC_{TOC*}	0.47 ± 0.03	0.34 ± 0.04	0.38 ± 0.05
RC_{COD*}	0.48 ± 0.08	0.41 ± 0.03	0.4 ± 0.1
RC_{CH*}	0.70 ± 0.02	0.57 ± 0.07	0.60 ± 0.06
RC_{Prot*}	0.69 ± 0.06	0.50 ± 0.05	0.54 ± 0.09
RC_{HA*}	0.47 ± 0.04	0.40 ± 0.03	0.47 ± 0.03

*CN: colour number; TOC: total organic carbon; COD: chemical oxygen demand; CH: carbohydrates; PROT: proteins; HA: humic acids; PES50: polyethersulphone, 50 kDa; PESH50: permanently hydrophilic polyethersulphone, 50 kDa; PAN: polyacrylonitrile, 50 kDa.

fouling will appear in the form of a gel-polarization layer. On the other hand, in hydrophobic membranes, the size of the irreversible adsorption layer increases until its thickness protects the hydrophobic surface from the adsorbed molecules, which generates higher values of irreversible fouling than in hydrophilic surfaces, and only after this limit is reached, the gel-polarization layer starts to form [59]. According to this, the behaviour of PES50 can be explained by its hydrophobic character, since more time was required for the initial membrane fouling to be fully occur, and the final concentration polarization layer needed less time to stabilise, thus starting to form at higher feed concentrations.

3.2.4. Atomic force microscopy

AFM images were taken from clean and fouled membranes in order to analyse the surface morphology (Fig. 4). The vertical profile of the membrane surface was represented by the colour intensity, with lighter colours indicating higher regions, and darker colours indicating depressions.

The surface of all the three clean membranes was clearly arranged in a "crest and valley" or "nodule and valley" pattern, originated by the random orientation and overlapping of the fibre structure [60]. This surface arrangement has also been observed by other authors when PES, PAN and polyamide membranes with flat-sheet, tubular and hollow-fibre geometries were used in ultrafiltration and nanofiltration processes [60–63]. The presence of valley-like formations is highly related to fouling, as foulant particles tend to deposit in these formations [64]. This fact was supported by the images of fouled membranes, where crest-like formations could no longer be seen, indicating that the valley-like regions had been clogged by foulants.

In addition to AFM imaging, membrane roughness was compared in terms of mean roughness (R_a [nm/μm]), root mean square roughness (rms), peak-to-peak distance (nm/μm), and surface skewness and

Table 4
Fitting parameters for the adjusted models.

		PES50	PESH50	PAN50
Hermia's models				
CPB	K_b (min^{-1})	$3.31{\cdot}10^{-2}$	5.29	$9.43{\cdot}10^{-2}$
	SSR	172,041.83	617,253.55	628,747.63
IPB	K_i (m^{-1})	$4.58{\cdot}10^{-3}$	$1.37{\cdot}10^{-1}$	$7.31{\cdot}10^{-3}$
	SSR	116,241.52	590,551.29	431,129.86
PPB	K_p (m^{-1})	$6.54{\cdot}10^{-4}$	$1.40{\cdot}10^{-3}$	$5.97{\cdot}10^{-4}$
	SSR	77,545.23	852,391.39	286,513.46
CF	K_c ($min{\cdot}m^{-2}$)	$1.45{\cdot}10^{-5}$	$4.42{\cdot}10^{-6}$	$3.86{\cdot}10^{-6}$
	SSR	32,776.51	255,336.20	129,005.00
Mehta's model				
$J_{\infty 1}$ (LMH)		46.05	114.16	116.08
α ($min-1$)		3.88	30.70	30.70
β ($min-1$)		$5.20{\cdot}10^{-2}$	$1.33{\cdot}10^{-2}$	$1.26{\cdot}10^{-2}$
SSR		700.38	1401.89	783.73

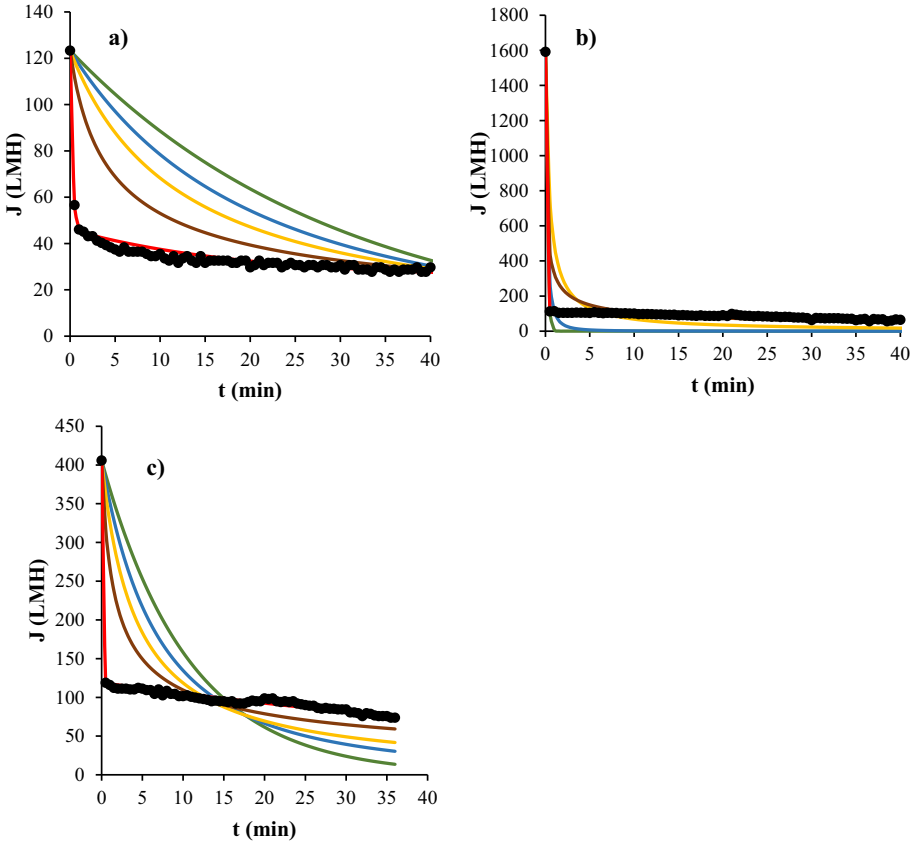

Fig. 3. Hermia's (complete pore blocking [▬], intermediate pore blocking [▬], partial pore blocking [▬] and cake formation [▬]) and Mehta's (▬) flux models for PES50 (a), PESH50 (b) and PAN50 (c) experimental fluxes (●).

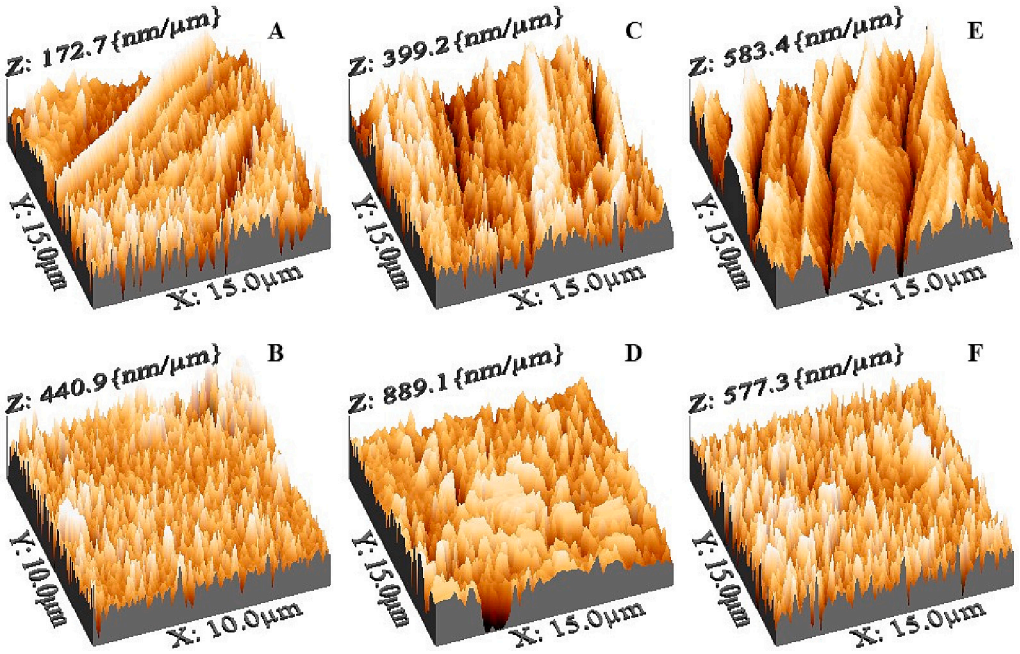

Fig. 4. AFM images of clean and fouled PES50 (A and B), PESH50 (C and D) and PAN50 (E and F) for membrane surface morphology analysis.

kurtosis in order to analyse its relationship with fouling (Table 5).

The loss of normalised flux was inversely related to R_a and rms values. In this sense, PES50, whose normalised flux decreased the least (77 %) during the ultrafiltration of the oxidised WAS, also showed the lowest R_a, rms and peak-to-peak distance values. Furthermore, the highest values were obtained with PESH50, which lost the highest proportion of normalised flux (96 %). The difference between normalised fluxes of PES50 and PAN50 was less marked than the roughness values may suggest, which could be explained based on their different hydrophilic properties (fouling allegedly increases with hydrophobicity [61]). The relationship between loss of normalised flux and R_a and rms values is in accordance with the existing literature, indicating that surface roughness plays a key role in flux loss [61,64–66]. As it was previously commented, in the initial stages of filtration, the particles tend to deposit in the "valley-like" formations of the membranes, clogging these depressed regions. Membranes with lower surface roughness present fewer "valley-like" formations on their surface, so the attachment of solute molecules is restricted [64]. The effect of this fewer presence of valley-like regions can be attended contrasting the roughness values from Table 5 with the images in Fig. 4: valley formations were more evident in PAN50 and PESH50 than in PES50, and the depth of the valleys was lower in the latter membrane, as it can be confirmed by the peak-to-peak distance.

Table 5
Membrane surface roughness parameters.

	Clean			Fouled		
	PES50	PESH50	PAN50	PES50	PESH50	PAN50
R_a [nm/µm]	23.0 ± 0.6	74 ± 5	67 ± 8	56 ± 15	164 ± 37	92 ± 6
rms	30.4 ± 0.9	94 ± 7	89 ± 5	41 ± 12	212 ± 47	119 ± 7
peak-to-peak distance [nm/µm]	142 ± 5	391 ± 32	365 ± 16	255 ± 59	918 ± 208	487 ± 26
Skewness	−0.23 ± 0.04	–	−0.08 ± 0.03	–	–	−0.05 ± 0.03
Kurtosis	3.35 ± 0.03	2.72 ± 0.05	2.8 ± 0.3	3.4 ± 0.4	2.89 ± 0.01	2.7 ± 0.1

As proved by the permeability tests and the AFM measurements, flux loss is a complex phenomenon, which depends on several factors, among which, the nature of the membrane surface (hydrophilic surfaces prevent fouling) and its rugosity (the higher the rugosity, the more space the solute molecules have for depositing) can be considered determinant.

3.3. Membrane molecular weight cut-off screening

3.3.1. Permeability tests

As PES was selected as the most suitable material for WAS fractioning (Section 3.2.2), the MWCO screening experiments were carried out with membranes made of this polymeric material (PES10 and PES3). The flux obtained with PES3 was extremely low (around 0.5 LMH on average), making this filtration unfeasible, and thus no data from this experiment are depicted. The fluxes obtained with PES10, PES50-10 and PES50-3 are shown in Fig. 5.

The highest flux obtained during the MWCO screening was achieved with PES50-10. However, the low rejection coefficients observed made this option unfeasible (Table 6). The highest rejections in terms of CN, TOC and COD were achieved with PES50-3. Nevertheless, in the case of the biomolecules, slightly differences were observed in rejections and rejection differences between PES10 and PES50-3.

Based on the rejection coefficients and the observed decrease in flux during the ultrafiltration of the oxidised WAS using PES10, as well as the permeates obtained from PES50 with PES10 and PES3, it can be concluded that the majority of molecules retained by the PES10 membrane can also be retained by the PES50 membrane. Therefore, coupling these two membranes would be redundant and unnecessary. This behaviour was in accordance with the work by Urrea et al. [67], where the effect of WO on the different molecular weight fractions of WAS was studied. They reported that, after a WO treatment at 190 °C and 90 min, the molecular weight of the majority of the present molecules was comprised in the ranges between 0 and 35 kDa (referred by Urrea et al. as low molecular weight molecules) and 35–150 kDa (medium molecular weight molecules). Moreover, hydrophobic molecules were also present due to the interactions with size-exclusion column. According to the results attained in this study, the sizes of the majority of the low molecular weight molecules were comprised between 0 and 10 kDa, and

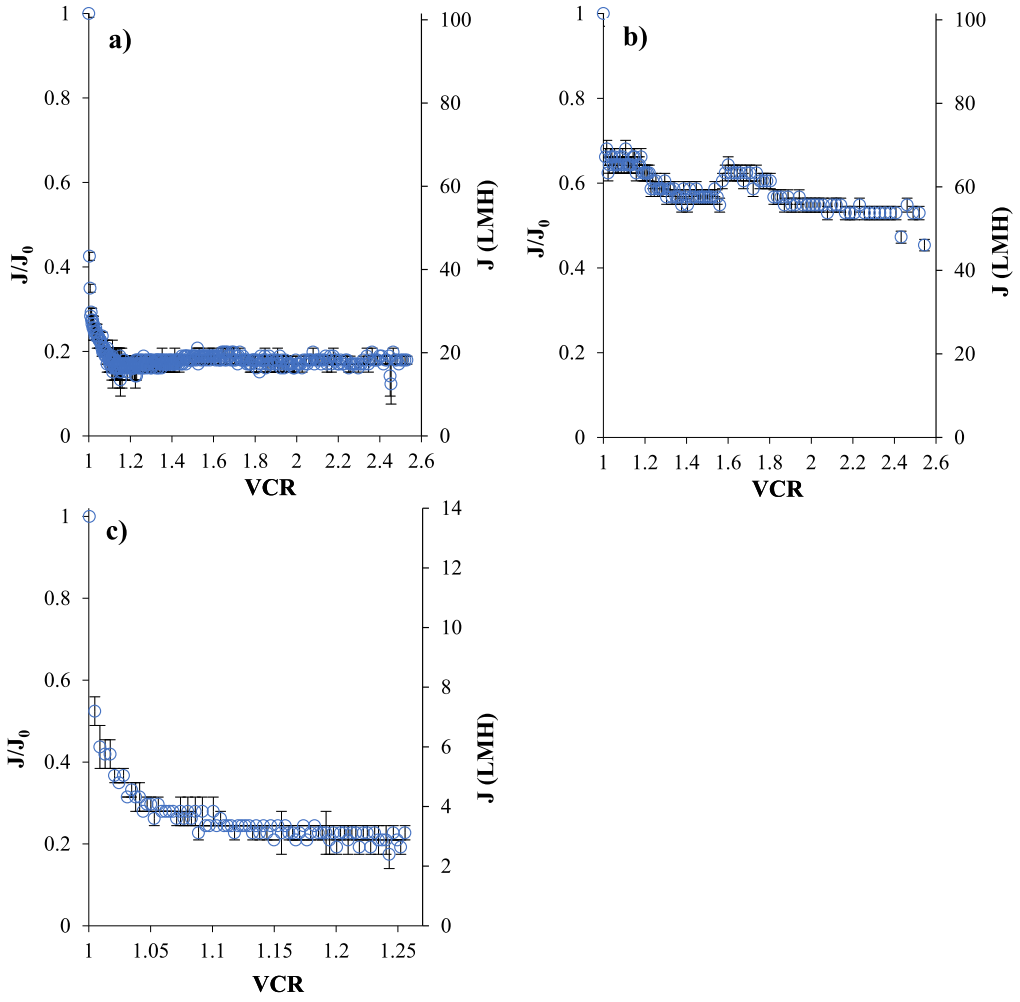

Fig. 5. Flux variation over VCR for the oxidised WAS filtration with PES10 (a) ($J_0 = 101.5 \pm 0.9$ L/m^{2}h), PES50-10 (b) ($J_0 = 102 \pm 3$ L/m^{2}h) and PES50-3 (c) ($J_0 = 13.72 \pm 0.01$ L/m^{2}h).

Table 6
Rejection coefficients obtained with PES10, PES50-10 and PES50-3.

	PES10	PES50-10	PES50-3
RC_{CN}	0.90 ± 0.01	0.35 ± 0.01	0.9942 ± 0.0009
RC_{TOC}	0.70 ± 0.16	0.17 ± 0.09	0.88 ± 0.01
RC_{COD}	0.60 ± 0.04	0.09 ± 0.04	0.66 ± 0.04
RC_{CH*}	0.79 ± 0.05	0.14 ± 0.05	0.83 ± 0.05
RC_{Prot*}	0.84 ± 0.09	0.21 ± 0.08	0.87 ± 0.06
RC_{HA*}	0.63 ± 0.05	0.15 ± 0.06	0.67 ± 0.06

*CH: carbohydrates; PROT: proteins; HA: humic acids.

the ones of the medium molecular weight molecules were above 50 kDa.

The resistance-in-series model (Fig. 6) showed that approximately half of the membrane fouling during the filtration with both PES10 and PES50-3 was irreversible, which contrast to the results obtained with PES50, where only 33 % of the fouling resistance was attributable to irreversible fouling. Moreover, a comparison between the values of the R_{rev} and the R_{irrev} obtained when filtering with PES50 and PES10 shows that no significant differences could be found between the values of reversible fouling, whereas the irreversible one of the PES10 membrane was around 2.5 times higher than that of the PES50 membrane. Thus, the additional flux decay observed between the filtration with PES10 and PES50 was exclusively due to an increase in irreversible fouling. It has been reported that irreversible fouling during the filtration of natural organic matter is primarily caused by the hydrophilic fraction of this organic matter [68–70]. Therefore, the additional irreversible fouling observed in this study is likely attributed to hydrophilic substances, presumably oxidised HA, since their rejection coefficients were lower than those of the other biomolecules, which suggests a lower average size. In this sense, several authors have reported that the oxidation of HA increased their hydrophilicity [71–74] by oxidizing benzene groups into different aldehydes and carboxylic acids [72,74]. After a subsequent reduction of the membrane MWCO to 3 kDa, the fouling profile remained similar (slightly more irreversible than reversible fouling), proving that the molecules retained by the PES50 membrane mainly caused reversible fouling. In this sense, Taniguchi et al. [57] compared the fouling of PES membranes with MWCOs from 10 to 1000 kDa during the UF of natural organic matter, and reported that membranes with lower MWCO (10 and 30 kDa) showed higher irreversible fouling, although fouling was mostly reversible in all cases.

3.3.2. *Fouling modelling*

The fitting of the studied fouling models to the experimental data corresponding to the filtrations with PES10, PES50-10 and PES50-3 is shown in Fig. 7.

Similarly to the filtration with the 50 kDa membranes, the best fitting Hermia's model was CF in the three filtrations. This results were in accordance to those reported by Peeva et al. [75] related to the ultrafiltration of humic acid solutions with PES membranes. However, as it was discussed in the previous section, the fitting showed that this model alone could not adequately explain the observed fouling tendency. In

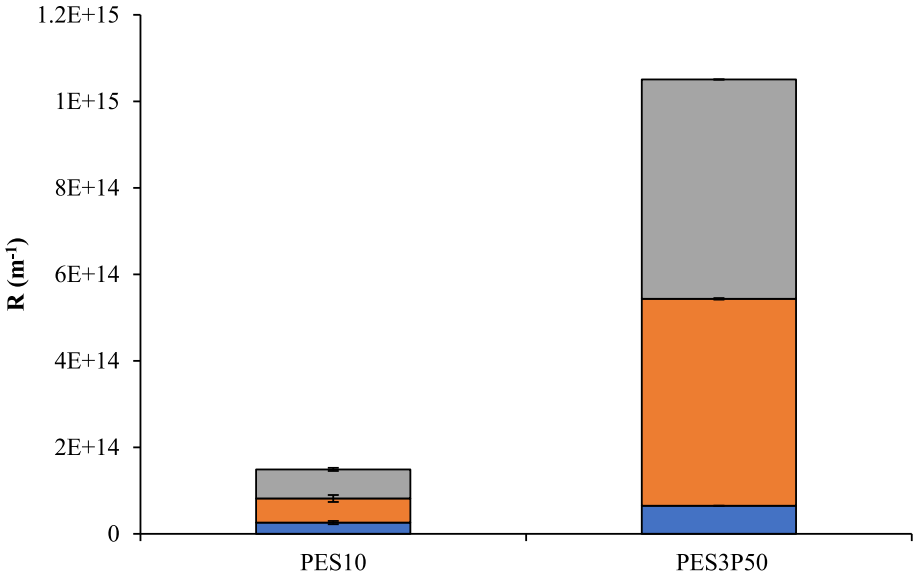

Fig. 6. R_m (■), R_{rev} (■) and R_{irrev} (■) after filtration with PES10 and PES50-3 membranes.

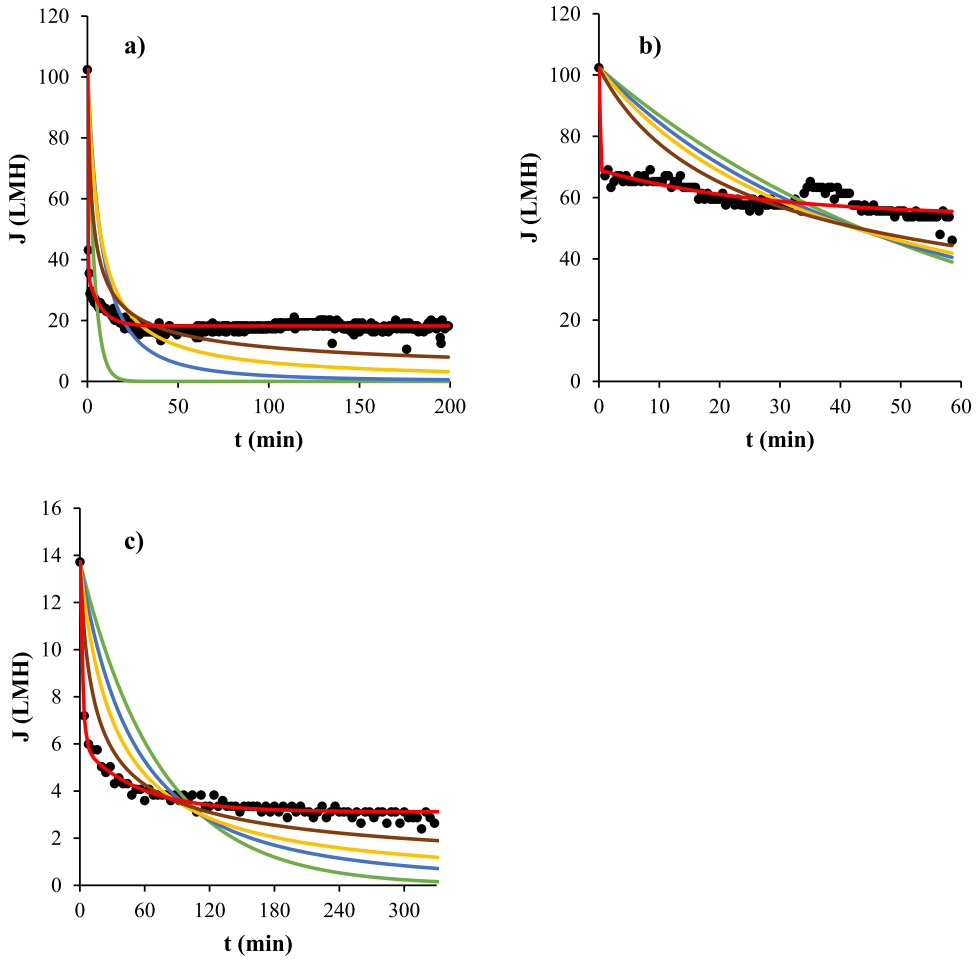

Fig. 7. Hermia's (complete pore blocking [■], intermediate pore blocking [■], partial pore blocking [■] and cake formation [■]) and Mehta's (■) flux models for PES10 (a), PES50-10 (b) and PES50-3 (c) experimental fluxes (●).

this case, the ultrafiltration of both the oxidised WAS with PES10 and the permeates obtained from PES50 with PES10 and PES3 suffered a proportionately higher irreversible fouling compared with the ultrafiltration of oxidised WAS with the PES50 membrane, which in all cases could be mainly attributed to PPB, as it was the second-best fitting Hermia's model (Table 7). The fact that PPB remained the main irreversible fouling mechanism in membranes with lower MWCO is in accordance with the literature. Thus, it has been reported that, when

Table 7
Fitting parameters for the adjusted models.

		PES10	PES50-10	PES50-3
Hermia's models				
CPB	K_b (min^{-1})	$2.68{\cdot}10^{-1}$	$1.65{\cdot}10^{-2}$	$1.36{\cdot}10^{-2}$
	SSR	129,413.22	37,272.70	596.61
IPB	K_i (m^{-1})	$1.26{\cdot}10^{-2}$	$1.99{\cdot}10^{-3}$	$5.52{\cdot}10^{-3}$
	SSR	108,753.21	33,256.49	372.75
PPB	K_p (m^{-1})	$1.51{\cdot}10^{-3}$	$2.41{\cdot}10^{-4}$	$2.32{\cdot}10^{-3}$
	SSR	73,673.60	29,768.57	227.88
CF	K_c ($min{\cdot}m^{-2}$)	$3.92{\cdot}10^{-5}$	$3.54{\cdot}10^{-6}$	$4.12{\cdot}10^{-4}$
	SSR	30,830.14	24,176.71	78.10
Mehta's model				
$J_{\infty 1}$ (LMH)		35.50	69.07	6.00
α (min^{-1})		4.03	36.27	$4.09{\cdot}10^{-1}$
β (min^{-1})		$1.40{\cdot}10^{-1}$	$3.69{\cdot}10^{-2}$	$1.92{\cdot}10^{-2}$
SSR		701.32	5599.28	3.95

filtering humic acids with PES membranes, a bigger pore size implied a greater fouling tendency towards pore narrowing instead of pore blocking [75]. This may indicate that the modification of the PES membrane to convert it into PESH enlarged its pores, which led to pore narrowing due to internal pore blocking as the major cause of its irreversible fouling.

Mehta's model fitted the data of the three filtrations perfectly. The high α value obtained for PES50-10 (Table 7) highlights the drastic initial membrane fouling. This may have occurred due to a fast pore clogging caused by the removal of molecules of higher molecular weight. These molecules, bigger than the pores, would have partially obstructed the access to the pores, thus starting to form the cake layer. Without the presence of the molecules higher than 50 kDa to favour the formation of this second barrier, smaller molecules would have entered the pores with much more ease at the beginning of the operation, clogging the pores in a faster way. This theory is supported by the fact that the β value obtained for PES50-10 was almost an order of magnitude smaller than that obtained for PES10, which indicates that the concentration polarization gradient and gel layer formation took more time to stabilise.

3.4. Infrared spectroscopy

In order to better understand the nature of the membrane materials used, as well as the interactions between the WAS and membranes of different materials and MWCOs, FTIR measurements were conducted on both the clean and fouled membranes.

All PES membranes and the PESH membrane exhibited the same FTIR profile (Figs. 8, A2 & A3), characterized by small bands at 3096 and 3068 cm^{-1}, corresponding to aromatic CH vibration; a small band at around 2964 cm^{-1}, caused by γ_a CH_3 asymmetric aliphatic stretching; two aromatic peaks at 1576 and 1484 cm^{-1} [76]; and peaks at 1409, 1296 and 1147 cm^{-1} indicating the presence of -S=O residues corresponding to the polysulfone material [77,78]. The band appearing at 1666 cm^{-1} could possibly be attributed to the presence of a preservative agent in the membrane [76].

The clean PAN membrane exhibited peaks at 2935 cm^{-1}, corresponding to alkane stretching, and at 2242 cm^{-1}, resulting from C≡N stretching. Additionally, it showed peaks in the 1500–1000 cm^{-1} region, indicative of alkanes. Furthermore, peaks at 1735 and 1661 cm^{-1} (Fig. A3) may be attributed to the C=C stretching of residual acrylonitrile monomers present in the membrane [78].

After filtration, a peak appeared in the fouled PES membranes at 1735–1712 cm^{-1} (Figs. 8 & A2), which is associated with C=O bonds [77,79]. The stretching at 1735 cm^{-1} corresponds to an aldehyde (which may originate from the alcohols present in carbohydrates, proteins and humic acids), while the peak at 1714 cm^{-1} to carboxylic acids (which are part of proteins, humic acids and fatty acids generated during the oxidation of organic matter [80]). Additionally, the spectra of all the fouled PES membranes showed a band at 1373 cm^{-1}, corresponding to

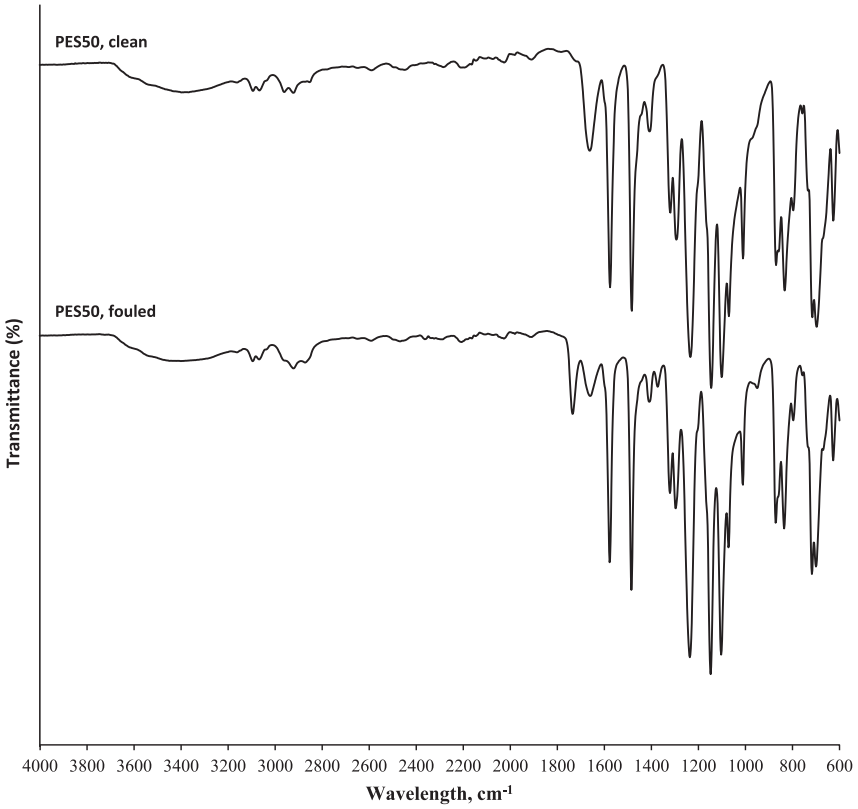

Fig. 8. FTIR spectra of PES50 membranes from 600 to 4000 cm^{-1}.

phenolic -OH groups [81], which are highly prevalent in humic substances [82]. These two signals were relatively weak in the PES50-10 spectrum, indicating lighter fouling of the membrane due to low retentions.

In addition to this, a band at 950 cm^{-1}, caused by alkene flexing, appeared only in the PES-based membranes that directly filtered the WAS (PES50, PESH50 and PES10), but not in the membranes that filtered WAS permeate (PES 50-10 and PES 50-3). This indicates that the molecule containing alkenes that interacted with the membrane surface was totally retained by the PES50 membrane.

PES50-3 exhibited the highest level of surface interactions after filtering, which is consistent with its predominant irreversible fouling. The aromatic bands at 3095 and 3068 cm^{-1} completely disappeared, while the aromatic peaks at 1578 and 1486 cm^{-1} nearly vanished. Similarly, the peaks at 1296, 1147 and 1071 cm^{-1}, corresponding to the sulfone group of the membrane, were significantly diminished. Furthermore, peaks associated to C—H bonds (at 830, 699 and 626 cm^{-1}) were no longer observable. This indicates that chemical (irreversible) interactions occurred between the foulants and both the aril and sulfone groups of the membrane.

The protein surface interaction with PESH50 membrane was confirmed by the presence of a peak at 1651 cm^{-1}, corresponding to Amine I [78], and a poorly resolved shoulder at 1550 cm^{-1} attributed to Amide II [76]. There is also a potential Amide I peak at 1640 cm^{-1} [75] that overlaps with the Amine I peak. [76].

The spectrum of the PAN membrane showed only minor changes after filtering the WAS, indicating that most of its fouling was reversible. However, there were noticeable increases in the intensity of certain peaks after filtration. Thus, the peak at 1661 cm^{-1}, as well as the peaks at 1040 and 1069 cm^{-1} showed an increased intensity, which are often correlated with carbohydrates [83]. Some bands corresponding to C—H bonds disappeared, indicating that foulant-membrane interactions occurred primarily in the alkane section of the polymer rather than the nitrile radical.

3.5. *Proposal of an integrated membrane process for biomolecule fractioning*

The results here obtained were used as a basis to propose an integrated membrane process to recover valuable biocompounds from WAS in order to valorise it in the context of circular economy. This process is based on size fractioning of oxidised WAS, thus obtaining two purified streams, one containing carbohydrates and proteins and the other one containing humic acids (Fig. 9).

PES membranes were found to be the suitable material for the ultrafiltration steps of the oxidised WAS due to their higher rejection coefficients and higher rejection differences between humic acids and the other biomolecules (proteins and carbohydrates). In this sense, a prefiltration with PES50 would be needed prior to the filtration with PES3 to prevent excessive fouling and the retentate of this prefiltration would be recirculated to the feed in order to keep the target biomolecules within the process. Then, the permeate of the PES50 prefiltration would be filtered with PES3. The concentration of the biomolecules at each ultrafiltration step was determined based on the rejection coefficients obtained in this study. Afterwards, a diafiltration step of the retentate of PES3 filtration would take place. The high rejection coefficients of proteins and carbohydrates (nearly 1), and the significant difference with the rejection coefficient of humic acid would allow a concentration and purification of carbohydrates and proteins thanks to this diafiltration, while humic acid would be washed in the permeate. Proteins and carbohydrates could then be separated by a chromatographic technique, such as expanded bed chromatography with an ion exchange resin [84] or immobilised metal affinity chromatography [85]. The permeate of PES3 filtrations, mainly consisting of a humic acid solution, could be concentrated by nanofiltration or reverse osmosis to obtain humic fertilizer, as reported by Li et al. [27,28,86]. It is important to note that the high proportion of irreversible fouling observed during the filtration with the PES3 membrane (51.5 % of total fouling) would pose challenges to the viability of the process. Therefore, future studies should focus on optimizing the filtration conditions, such as investigation the critical flux [87] or employing techniques like backwashing, air scouring [88], membrane patterning [87], and surface coating [89], among others.

4. Conclusions

The screening tests of membrane material showed that PES was found to be the best material for the fractionation of humic acids and proteins from oxidised WAS, since higher rejection coefficients and differences between these biomolecules were achieved after filtering with PES50, although lower fluxes were obtained compared to PESH50 and PAN50 membranes. In particular, the rejection coefficients attained with the PES50 membrane were 0.70 ± 0.02 for carbohydrates, 0.69 ± 0.06 for proteins and 0.47 ± 0.04 for humic acids (with a difference of 23 % and 22 % comparing carbohydrates and proteins selectivities with humic acids, respectively).

The main fouling mechanism can be considered CF in all cases, but with an important irreversible component in PES50 and especially in PESH50, as shown by the resistance-in-series model. Thanks to AFM imaging, the key role of the arrangement of the surface of the membranes and their mean roughness in flux loss was proven in all cases. The screening tests of membrane MWCO showed that both the 50 kDa and

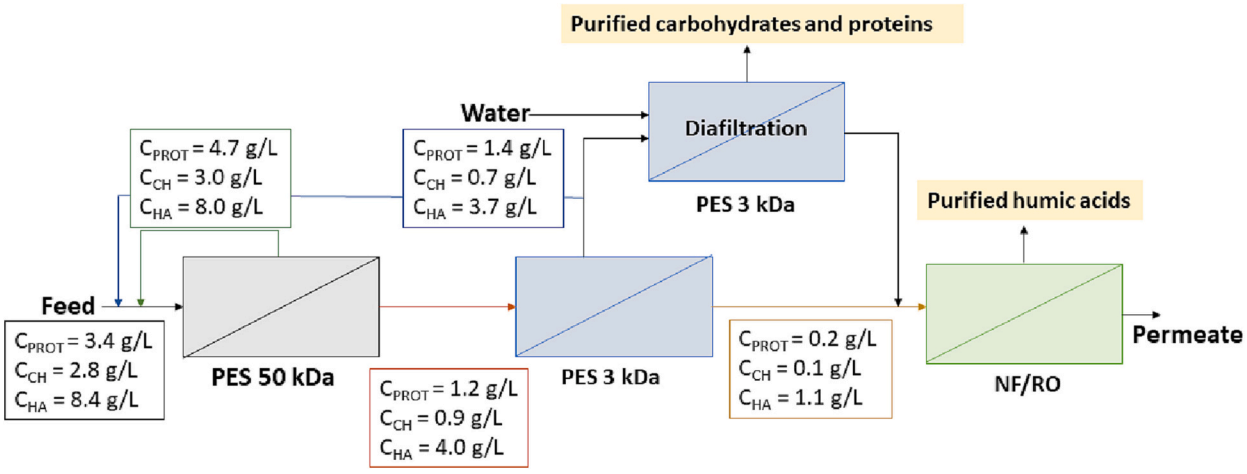

Fig. 9. Size fractioning results and proposal for carbohydrates (CH) and proteins (P), and humic acids (HA) purification.

10 kDa PES membranes exhibited high biomolecule retentions, reaching rates of up to 84 %. However, when the permeate from the PES50 filtration was subsequently filtered using the PES10 membrane, lower retentions (up to 21 %) were observed. Therefore, in order to fractionate the oxidised WAS, the use of PES50 and PES3 membranes would be more adequate, the filtration with the PES50 one being necessary to attain acceptable fluxes with the PES3 membrane. Excellent retentions of 0.83 $\pm$ 0.05 and 0.87 $\pm$ 0.06 for carbohydrates and proteins, respectively, as well as a difference of 20 % in selectivity between proteins and humic acids, were obtained with the PES3 membranes, although its efficiency was affected by a significant irreversible fouling (51.5 % of total fouling). Although CF was still the main fouling mechanism, a reduction of the membrane MWCO derived in a more irreversible fouling, presumably due to particle pore blocking.

Based on the results here obtained, an integrated process of membrane filtration was proposed in order to obtain purified streams of humic acids, carbohydrates and proteins. Future works should indicate the efficiency of the suggested steps of diafiltration and nanofiltration/reverse osmosis, and evaluate how affects the higher concentration of humic acids in the WAS in comparison with proteins and carbohydrates on the effective separation of these biomolecules.

Declaration of competing interest

The authors declare that they have no known competing financial interests or personal relationships that could have appeared to influence the work reported in this paper.

Data availability

Data will be made available on request.

Acknowledgements

The authors are grateful for the financial support from the Spanish Ministry of Science, Innovation and Universities through the projects MCIU-19-RTI2018-094218-B-I00 and MCIU-22-PID2021-125942OB-I00. Authors also want to acknowledge the Employment, Industry and Tourism Office of the Principality of Asturias, Spain, for their financial support through the project AYUD/2021/51041. The author Daniel Núñez thanks the Principality of Asturias, Spain, for their financial support through the Severo Ochoa scholarship n^{o} BP19-093.

Appendix A. Supplementary data

Supplementary data to this article can be found online at https://doi.org/10.1016/j.jwpe.2023.104086.

References

[1] S. Venkata Mohan, G.N. Nikhil, P. Chiranjeevi, C. Nagendranatha Reddy, M. V. Rohit, A.N. Kumar, O. Sarkar, Waste biorefinery models towards sustainable circular bioeconomy: critical review and future perspectives, Bioresour. Technol. 215 (2016) 2–12, https://doi.org/10.1016/j.biortech.2016.03.130.
[2] V. De Buck, M. Polanska, J. Van Impe, Modeling biowaste biorefineries: a review, Front. Sustain. Food Syst. 4 (2020) 11, https://doi.org/10.3389/fsufs.2020.00011.
[3] Market Study Report, Global Biorefinery Market Value to Surpass USD 52680, 2021.
[4] A.P. Bora, D.P. Gupta, K.S. Durbha, Sewage sludge to bio-fuel: a review on the sustainable approach of transforming sewage waste to alternative fuel, Fuel. 259 (2020), 116262, https://doi.org/10.1016/j.fuel.2019.116262.
[5] A. Raheem, V.S. Sikarwar, J. He, W. Dastyar, D.D. Dionysiou, W. Wang, M. Zhao, Opportunities and challenges in sustainable treatment and resource reuse of sewage sludge: a review, Chem. Eng. J. 337 (2018) 616–641, https://doi.org/10.1016/j.cej.2017.12.149.
[6] B. Cieślik, P. Konieczka, A review of phosphorus recovery methods at various steps of wastewater treatment and sewage sludge management. The concept of "no solid waste generation" and analytical methods, J. Clean. Prod. 142 (2017) 1728–1740, https://doi.org/10.1016/j.jclepro.2016.11.116.
[7] W. Liu, H. Yang, J. Ye, J. Luo, Y.Y. Li, J. Liu, Short-chain fatty acids recovery from sewage sludge via acidogenic fermentation as a carbon source for denitrification: a review, Bioresour. Technol. 311 (2020), 123446, https://doi.org/10.1016/j.biortech.2020.123446.
[8] M.N. Siddiquee, S. Rohani, Lipid extraction and biodiesel production from municipal sewage sludges: a review, Renew. Sust. Energ. Rev. 15 (2011) 1067–1072, https://doi.org/10.1016/J.RSER.2010.11.029.
[9] K. Xiao, Y. Zhou, Protein recovery from sludge: a review, J. Clean. Prod. 249 (2020), 119373, https://doi.org/10.1016/j.jclepro.2019.119373.
[10] P. Supaporn, H.V. Ly, S.S. Kim, S.H. Yeom, Bio-oil production using residual sewage sludge after lipid and carbohydrate extraction, Environ. Eng. Res. 24 (2019) 202–210, https://doi.org/10.4491/eer.2017.178.
[11] D. Núñez, P. Oulego, S. Collado, F.A. Riera, M. Díaz, Separation and purification techniques for the recovery of added-value biocompounds from waste activated sludge. A review, Resour. Conserv. Recycl. 182 (2022), 106327, https://doi.org/10.1016/j.resconrec.2022.106327.
[12] J.L. Urrea, S. Collado, P. Oulego, M. Díaz, Formation and degradation of soluble biopolymers during wet oxidation of sludge, ACS Sustain. Chem. Eng. 5 (2017) 3011–3018, https://doi.org/10.1021/ACSSUSCHEMENG.6B02664.
[13] G.P. Sheng, J. Xu, W.H. Li, H.Q. Yu, Quantification of the interactions between Ca2+, Hg2+ and extracellular polymeric substances (EPS) of sludge, Chemosphere. 93 (2013) 1436–1441, https://doi.org/10.1016/J.CHEMOSPHERE.2013.07.076.
[14] L. Wei, K. Wang, X. Kong, G. Liu, S. Cui, Q. Zhao, F. Cui, Application of ultrasonication, acid precipitation and membrane filtration for co-recovery of protein and humic acid from sewage sludge, Front. Environ. Sci. Eng. 10 (2016) 327–335, https://doi.org/10.1007/s11783-014-0763-9.
[15] J. Hwang, L. Zhang, S. Seo, Y.W. Lee, D. Jahng, Protein recovery from excess sludge for its use as animal feed, Bioresour. Technol. 99 (2008) 8949–8954, https://doi.org/10.1016/j.biortech.2008.05.001.
[16] A.P. Bhat, P.R. Gogate, Cavitation-based pre-treatment of wastewater and waste sludge for improvement in the performance of biological processes: a review, J. Environ. Chem. Eng. 9 (2021), 104743, https://doi.org/10.1016/J.JECE.2020.104743.
[17] M. Pervaiz, M. Sain, Protein extraction from secondary sludge of paper mill wastewater and its utilization as a wood adhesive, BioResources. 6 (2011) 961–970.
[18] B. Otieno, S. Apollo, J. Kabuba, B. Naidoo, G. Simate, A. Ochieng, Ozonolysis pre-treatment of waste activated sludge for solubilization and biodegradability enhancement, J. Environ. Chem. Eng. 7 (2019), 102945, https://doi.org/10.1016/J.JECE.2019.102945.
[19] M. García, J.L. Urrea, S. Collado, P. Oulego, M. Díaz, Protein recovery from solubilized sludge by hydrothermal treatments, Waste Manag. 67 (2017) 278–287, https://doi.org/10.1016/J.WASMAN.2017.05.051.
[20] E. Slavik, R. Galessi, A. Rapisardi, R. Salvetti, P. Bonzagni, G. Bertanza, L. Menoni, D. Orhon, S. Sözen, Wet oxidation as an advanced and sustainable technology for sludge treatment and management: results from research activities and industrial-scale experiences, Dry. Technol. 33 (2015) 1309–1317, https://doi.org/10.1080/07373937.2015.1036282.
[21] L. Wei, J. Li, M. Xue, S. Wang, Q. Li, K. Qin, J. Jiang, J. Ding, Q. Zhao, Adsorption behaviors of Cu2+, Zn2+ and Cd2+ onto proteins, humic acid, and polysaccharides extracted from sludge EPS: sorption properties and mechanisms, Bioresour. Technol. 291 (2019), 121868, https://doi.org/10.1016/j.biortech.2019.121868.
[22] I. Sargin, G. Arslan, M. Erzengin, Interactions of bovine serum albumin with humic acid-Cu(II) aggregates in poly(hydroxyethylmethacrylate) cryogel column, J. Taiwan Inst. Chem. Eng. 63 (2016) 101–106, https://doi.org/10.1016/j.jtice.2016.03.032.
[23] T.A. Saleh, V.K. Gupta, An overview of membrane science and technology, in: Nanomater. Polym. Membr, Elsevier, 2016, pp. 1–23, https://doi.org/10.1016/B978-0-12-804703-3.00001-2.
[24] D.M. Kanani, W.H. Fissell, S. Roy, A. Dubnisheva, A. Fleischman, A.L. Zydney, Permeability-selectivity analysis for ultrafiltration: effect of pore geometry, J. Membr. Sci. 349 (2010) 405–410, https://doi.org/10.1016/j.memsci.2009.12.003.
[25] A. Behboudi, Y. Jafarzadeh, R. Yegani, Enhancement of antifouling and antibacterial properties of PVC hollow fiber ultrafiltration membranes using pristine and modified silver nanoparticles, J. Environ. Chem. Eng. 6 (2018) 1764–1773, https://doi.org/10.1016/J.JECE.2018.02.031.
[26] H.J. Tanudjaja, A. Anantharaman, A.Q.Q. Ng, Y. Ma, M.B. Tanis-Kanbur, A. L. Zydney, J.W. Chew, A review of membrane fouling by proteins in ultrafiltration and microfiltration, J. Water Process Eng. 50 (2022), 103294, https://doi.org/10.1016/j.jwpe.2022.103294.
[27] H. Li, Y. Li, S. Zou, C. Li, Extracting humic acids from digested sludge by alkaline treatment and ultrafiltration, J. Mater. Cycles Waste Manag. 16 (2014) 93–100, https://doi.org/10.1007/s10163-013-0153-6.
[28] H. Li, Y. Li, Y. Jin, S. Zou, C. Li, Recovery of sludge humic acids with alkaline pretreatment and its impact on subsequent anaerobic digestion, J. Chem. Technol. Biotechnol. 89 (2014) 707–713, https://doi.org/10.1002/jctb.4173.
[29] L. Pola, L. Fernández-García, S. Collado, P. Oulego, M. Díaz, Macronutrient solubilisation during hydrothermal treatment of sewage sludge, J. Water Process Eng. 43 (2021), 102270, https://doi.org/10.1016/J.JWPE.2021.102270.
[30] L. Pola, S. Collado, P. Oulego, M. Díaz, Production of carboxylic acids from the non-lignin residue of black liquor by hydrothermal treatments, Bioresour. Technol. 284 (2019) 105–114, https://doi.org/10.1016/j.biortech.2019.03.066.
[31] S. Collado, D. Núñez, P. Oulego, F.A. Riera, M. Díaz, Effect of landfill leachate ageing on ultrafiltration performance and membrane fouling behaviour, J. Water Process Eng. 36 (2020), https://doi.org/10.1016/j.jwpe.2020.101291.

[32] J. Hermia, Constant pressure blocking filtration laws-application topower-law non-Newtonian fluids, Trans. Inst. Chem. Eng. 60 (1982) 183–187.
[33] Z.F. Cui, H.S. Muralidhara, Membrane Technology, Elsevier, 2010, https://doi.org/10.1016/C2009-0-19129-8.
[34] B. Mehta, Processing of Model Compositional Whey Solutions with Pressure Driven Membranes, Ohio State University, 1973.
[35] M. Mondor, B. Girard, C. Moresoli, Modeling flux behavior for membrane filtration of apple juice, Food Res. Int. 33 (2000) 539–548, https://doi.org/10.1016/S0963-9969(00)00089-2.
[36] I. Horcas, R. Fernández, J.M. Gómez-Rodríguez, J. Colchero, J. Gómez-Herrero, A. M. Baro, WSxM: a software for scanning probe microscopy and a tool for nanotechnology, Rev. Sci. Instrum. 78 (2007), 013705, https://doi.org/10.1063/1.2432410.
[37] A.W. Mohammad, N. Hilal, L.Y. Pei, I.N.H. Mohd Amin, R. Raslan, Atomic force microscopy as a tool for asymmetric polymeric membrane characterization, Sains Malaysiana 40 (2011) 237–244.
[38] R. Sudha, Measures of skewness and kurtosis, Res. Biostat. Nurses 200 (2017) 412, https://doi.org/10.5005/jp/books/13016_16.
[39] B. Frølund, R. Palmgren, K. Keiding, P.H. Nielsen, Extraction of extracellular polymers from activated sludge using a cation exchange resin, Water Res. 30 (1996) 1749–1758, https://doi.org/10.1016/0043-1354(95)00323-1.
[40] M. Dubois, K.A. Gilles, J.K. Hamilton, P.A. Rebers, F. Smith, Colorimetric method for determination of sugars and related substances, Anal. Chem. 28 (1956) 350–356, https://doi.org/10.1021/ac60111a017.
[41] APHA, AWWA, WEF, APHA, AWWA, WEF, Standard methods for examination of water and wastewater, An. Hidrol. Médica. 5 (2012) 185–186, https://doi.org/10.5209/rev_ANHM.2012.v5.n2.40440.
[42] K.Y. Law, Definitions for hydrophilicity, hydrophobicity, and superhydrophobicity: getting the basics right, J. Phys. Chem. Lett. 5 (2014) 686–688, https://doi.org/10.1021/jz402762h.
[43] A.V.R. Reddy, H.R. Patel, Chemically treated polyethersulfone/polyacrylonitrile blend ultrafiltration membranes for better fouling resistance, Desalination. 221 (2008) 318–323, https://doi.org/10.1016/j.desal.2007.01.089.
[44] C. Zhao, J. Xue, F. Ran, S. Sun, Modification of polyethersulfone membranes - a review of methods, Prog. Mater. Sci. 58 (2013) 76–150, https://doi.org/10.1016/j.pmatsci.2012.07.002.
[45] V. Vatanpour, M. Mehrabi, M. Masteri-Farahani, A.H. Behroozi, M. Niakan, I. Koyuncu, Sulfonic acid functionalized dendrimer-grafted cellulose as a charge and hydrophilic modifier of cellulose acetate membranes in removal of inorganic and organic pollutants, J. Water Process Eng. 50 (2022), 103307, https://doi.org/10.1016/j.jwpe.2022.103307.
[46] O. Al-Akoum, L.H. Ding, M.Y. Jaffrin, Microfiltration and ultrafiltration of UHT skim milk with a vibrating membrane module, Sep. Purif. Technol. 28 (2002) 219–234, https://doi.org/10.1016/S1383-5866(02)00076-X.
[47] L.E. Fratila-Apachitei, M.D. Kennedy, J.D. Linton, I. Blume, J.C. Schippers, Influence of membrane morphology on the flux decline during dead-end ultrafiltration of refinery and petrochemical waste water, J. Membr. Sci. 182 (2001) 151–159, https://doi.org/10.1016/S0376-7388(00)00557-3.
[48] L. Li, L. Ding, Z. Tu, Y. Wan, D. Clausse, J.L. Lanoisellé, Recovery of linseed oil dispersed within an oil-in-water emulsion using hydrophilic membrane by rotating disk filtration system, J. Membr. Sci. 342 (2009) 70–79, https://doi.org/10.1016/J.MEMSCI.2009.06.023.
[49] M. Al-Maas, A. Hussain, J. Minier Matar, D. Ponnamma, M.K. Hassan, M. Al Ali Al-Maadeed, K. Alamgir, S. Adham, Validation and application of a membrane filtration evaluation protocol for oil-water separation, J. Water Process Eng. 43 (2021), 102185, https://doi.org/10.1016/J.JWPE.2021.102185.
[50] S.F.E. Boerlage, M.D. Kennedy, M.R. Dickson, D.E.Y. El-Hodali, J.C. Schippers, The modified fouling index using ultrafiltration membranes (MFI-UF): characterisation, filtration mechanisms and proposed reference membrane, J. Membr. Sci. 197 (2002) 1–21, https://doi.org/10.1016/S0376-7388(01)00618-4.
[51] Q. Yang, J. Luo, S. Guo, X. Hang, X. Chen, Y. Wan, Threshold flux in concentration mode: fouling control during clarification of molasses by ultrafiltration, J. Membr. Sci. 586 (2019) 130–139, https://doi.org/10.1016/J.MEMSCI.2019.05.063.
[52] M. Cifuentes-Cabezas, C. Carbonell-Alcaina, M.C. Vincent-Vela, J.A. Mendoza-Roca, S. Álvarez-Blanco, Comparison of different ultrafiltration membranes as first step for the recovery of phenolic compounds from olive-oil washing wastewater, Process. Saf. Environ. Prot. 149 (2021) 724–734, https://doi.org/10.1016/J.PSEP.2021.03.035.
[53] I.S. Chang, S.O. Bag, C.H. Lee, Effects of membrane fouling on solute rejection during membrane filtration of activated sludge, Process Biochem. 36 (2001) 855–860, https://doi.org/10.1016/S0032-9592(00)00284-3.
[54] G. Di Bella, D. Di Trapani, A brief review on the resistance-in-series model in membrane bioreactors (MBRs), Membranes (Basel). 9 (2019) 24, https://doi.org/10.3390/membranes9020024.
[55] A.R. Costa, M.N. de Pinho, M. Elimelech, Mechanisms of colloidal natural organic matter fouling in ultrafiltration, J. Membr. Sci. 281 (2006) 716–725, https://doi.org/10.1016/J.MEMSCI.2006.04.044.
[56] W. Guo, H.H. Ngo, J. Li, A mini-review on membrane fouling, Bioresour. Technol. 122 (2012) 27–34, https://doi.org/10.1016/j.biortech.2012.04.089.
[57] M. Taniguchi, J.E. Kilduff, G. Belfort, Modes of natural organic matter fouling during ultrafiltration, Environ. Sci. Technol. 37 (2003) 1676–1683, https://doi.org/10.1021/es020555p.
[58] L. Bai, H. Wu, J. Ding, A. Ding, X. Zhang, N. Ren, G. Li, H. Liang, Cellulose nanocrystal-blended polyethersulfone membranes for enhanced removal of natural organic matter and alleviation of membrane fouling, Chem. Eng. J. 382 (2020), 122919, https://doi.org/10.1016/J.CEJ.2019.122919.
[59] A.N. Cherkasov, S.V. Tsareva, A.E. Polotsky, Selective properties of ultrafiltration membranes from the standpoint of concentration polarization and adsorption phenomena, J. Membr. Sci. 104 (1995) 157–164, https://doi.org/10.1016/0376-7388(95)00022-5.
[60] S. Rajesh, Y. Zhao, H. Fong, T.J. Menkhaus, Polyacrylonitrile nanofiber membranes modified with ionically crosslinked polyelectrolyte multilayers for the separation of ionic impurities, Nanoscale. 8 (2016) 18376–18389, https://doi.org/10.1039/C6NR06295D.
[61] N. Hilal, H. Al-Zoubi, N.A. Darwish, A.W. Mohammad, Characterisation of nanofiltration membranes using atomic force microscopy, Desalination. 177 (2005) 187–199, https://doi.org/10.1016/j.desal.2004.12.008.
[62] H.R. Lohokare, M.R. Muthu, G.P. Agarwal, U.K. Kharul, Effective arsenic removal using polyacrylonitrile-based ultrafiltration (UF) membrane, J. Membr. Sci. 320 (2008) 159–166, https://doi.org/10.1016/J.MEMSCI.2008.03.068.
[63] M.S. Muhamad, M.R. Salim, W.-J. Lau, Surface modification of SiO2 nanoparticles and its impact on the properties of PES-based hollow fiber membrane, RSC Adv. 5 (2015) 58644–58654, https://doi.org/10.1039/C5RA07527K.
[64] K. Boussu, B. Van Der Bruggen, A. Volodin, J. Snauwaert, C. Van Haesendonck, C. Vandecasteele, Roughness and hydrophobicity studies of nanofiltration membranes using different modes of AFM, J. Colloid Interface Sci. 286 (2005) 632–638, https://doi.org/10.1016/J.JCIS.2005.01.095.
[65] G. Makdissy, J.P. Croué, H. Buisson, G. Amy, B. Legube, Organic matter fouling of ultrafiltration membranes, Water Supply 3 (2003) 175–182, https://doi.org/10.2166/WS.2003.0164.
[66] Y.L. Thuyavan, N. Anantharaman, G. Arthanareeswaran, A.F. Ismail, Impact of solvents and process conditions on the formation of polyethersulfone membranes and its fouling behavior in lake water filtration, J. Chem. Technol. Biotechnol. 91 (2016) 2568–2581, https://doi.org/10.1002/JCTB.4846.
[67] J.L. Urrea, S. Collado, P. Oulego, M. Díaz, Effect of wet oxidation on the fingerprints of polymeric substances from an activated sludge, Water Res. 105 (2016) 282–290, https://doi.org/10.1016/J.WATRES.2016.09.004.
[68] H. Yamamura, K. Okimoto, K. Kimura, Y. Watanabe, Hydrophilic fraction of natural organic matter causing irreversible fouling of microfiltration and ultrafiltration membranes, Water Res. 54 (2014) 123–136, https://doi.org/10.1016/j.watres.2014.01.024.
[69] K. Kimura, H. Yamamura, Y. Watanabe, Irreversible fouling in MF/UF membranes caused by Natural Organic Matters (NOMs) isolated from different origins, Sep. Sci. Technol. 41 (2006) 1331–1344, https://doi.org/10.1080/01496390600634665.
[70] Y. Bessiere, B. Jefferson, E. Goslan, P. Bacchin, Effect of hydrophilic/hydrophobic fractions of natural organic matter on irreversible fouling of membranes, Desalination. 249 (2009) 182–187, https://doi.org/10.1016/j.desal.2008.12.047.
[71] L. Doskočil, L. Grasset, D. Válková, M. Pekař, Hydrogen peroxide oxidation of humic acids and lignite, Fuel. 134 (2014) 406–413, https://doi.org/10.1016/J.FUEL.2014.06.011.
[72] L. Zhou, L. Yuan, B. Zhao Id, Y. Li, Z. Lin, Structural Characteristics of Humic Acids Derived From Chinese Weathered Coal Under Different Oxidizing Conditions, 2019, https://doi.org/10.1371/journal.pone.0217469.
[73] R. Zhu, A.J. Diaz, Y. Shen, F. Qi, X. Chang, D.P. Durkin, Y. Sun, S.D. Solares, D. Shuai, Mechanism of humic acid fouling in a photocatalytic membrane system, J. Membr. Sci. 563 (2018) 531–540, https://doi.org/10.1016/j.memsci.2018.06.017.
[74] T. Zeng, C.J. Wilson, W.A. Mitch, Effect of chemical oxidation on the sorption tendency of dissolved organic matter to a model hydrophobic surface, Environ. Sci. Technol. 48 (2014) 5118–5126, https://doi.org/10.1021/es405257b.
[75] P.D. Peeva, A.E. Palupi, M. Ulbricht, Ultrafiltration of humic acid solutions through unmodified and surface functionalized low-fouling polyethersulfone membranes – effects of feed properties, molecular weight cut-off and membrane chemistry on fouling behavior and cleanability, Sep. Purif. Technol. 81 (2011) 124–133, https://doi.org/10.1016/J.SEPPUR.2011.07.005.
[76] S. Belfer, R. Fainchtain, Y. Purinson, O. Kedem, Surface characterization by FTIR-ATR spectroscopy of polyethersulfone membranes-unmodified, modified and protein fouled, J. Membr. Sci. 172 (2000) 113–124.
[77] S. Acarer, İ. Pir, M. Tüfekci, G. Türkoğlu Demirkol, N. Tüfekci, Manufacturing and characterisation of polymeric membranes for water treatment and numerical investigation of mechanics of nanocomposite membranes, Polym. 13 (2021) 1661, https://doi.org/10.3390/POLYM13101661.
[78] Merck KGaA, IR Spectrum Table. https://www.sigmaaldrich.com/ES/en/technical-documents/technical-article/analytical-chemistry/photometry-and-reflectometry/ir-spectrum-table, 2023 (accessed June 5, 2023).
[79] R.E. Farsani, S. Raissi, A. Shokuhfar, A. Sedghi, FT-IR study of stabilized pan fibers for fabrication of carbon fibers, World Acad. Sci. Eng. Technol. 38 (2009) 434–437.
[80] S. Baroutian, A.M. Smit, J. Andrews, B. Young, D. Gapes, Hydrothermal degradation of organic matter in municipal sludge using non-catalytic wet oxidation, Chem. Eng. J. 260 (2015) 846–854, https://doi.org/10.1016/j.cej.2014.09.063.
[81] C.M. Popescu, C. Vasile, M.C. Popescu, G. Singurel, V.I. Popa, B.S. Munteanu, Analytical methods for lignin characterization. II. Spectroscopic studies, Cellul. Chem. Technol. 40 (2006) 597–621.
[82] M. Banach-Szott, B. Debska, Content of phenolic compounds in fulvic and humic acid fractions of forest soils, polish, J. Environ. Stud. 17 (2008) 463–472.
[83] L. Zhu, H. ying Qi, M. Le Lv, Y. Kong, Y.W. Yu, X.Y. Xu, Component analysis of extracellular polymeric substances (EPS) during aerobic sludge granulation using FTIR and 3D-EEM technologies, Bioresour. Technol. 124 (2012) 455–459, https://doi.org/10.1016/j.biortech.2012.08.059.
[84] A.-K. Barnfield Frej, R. Hjorth, Å. Hammarström, Pilot scale recovery of recombinant annexin V from unclarified escherichia coli homogenate using

expanded bed adsorption, Biotechnol. Bioeng. 44 (1994) 922–929, https://doi.org/10.1002/bit.260440808.
[85] H. Block, B. Maertens, A. Spriestersbach, N. Brinker, J. Kubicek, R. Fabis, J. Labahn, F. Schäfer, Chapter 27 Immobilized-Metal Affinity Chromatography (IMAC). A Review, in: Methods Enzymol, 2009, pp. 439–473, https://doi.org/10.1016/S0076-6879(09)63027-5.
[86] H. Li, Y. Jin, Y. Nie, Application of alkaline treatment for sludge decrement and humic acid recovery, Bioresour. Technol. 100 (2009) 6278–6283, https://doi.org/10.1016/j.biortech.2009.07.022.
[87] S.H. Maruf, A.R. Greenberg, J. Pellegrino, Y. Ding, Critical Flux of Surface-patterned Ultrafiltration Membranes During Cross-flow Filtration of Colloidal Particles, 2014, https://doi.org/10.1016/j.memsci.2014.07.071.
[88] X. Tang, T. Guo, H. Chang, X. Yue, J. Wang, H. Yu, B. Xie, X. Zhu, G. Li, H. Liang, Membrane Fouling Alleviation by Chemically Enhanced Backwashing in Treating Algae-Containing Surface Water: From Bench-Scale to Full-Scale Application, (n. d.). doi:https://doi.org/10.1016/j.eng.2021.01.013.
[89] Y. Bhoj, M. Tharmavaram, D. Rawtani, A comprehensive approach to antifouling strategies in desalination, marine environment, and wastewater treatment, Chem. Phys. Impact. 2 (2021), 100008, https://doi.org/10.1016/j.chphi.2020.100008.